Acetic acid conversion to ketene on Cu<inf>2</inf>O(1 0 0): Reaction mechanism deduced from experimental observations and theoretical

Downloaded from: https://research.chalmers.se, 2025-12-04 20:21 UTC

Citation for the original published paper (version of record):
Tissot, H., Halldin Stenlid, J., Wang, C. et al (2021). Acetic acid conversion to ketene on Cu<inf>2</inf>O(1 0 0): Reaction mechanism deduced from experimental observations and theoretical computations. Journal of Catalysis, 402: 154-165. http://dx.doi.org/10.1016/j.jcat.2021.08.022

N.B. When citing this work, cite the original published paper.

research.chalmers.se offers the possibility of retrieving research publications produced at Chalmers University of Technology. It covers all kind of research output: articles, dissertations, conference papers, reports etc. since 2004. research.chalmers.se is administrated and maintained by Chalmers Library

(article starts on next page)

Journal of Catalysis 402 (2021) 154–165

Contents lists available at ScienceDirect

Journal of Catalysis

journal homepage: www.elsevier.com/locate/jcat

Acetic acid conversion to ketene on $Cu_2O(100)$: Reaction mechanism deduced from experimental observations and theoretical computations

H. Tissot [a], J. Halldin Stenlid [f], C. Wang [a], M. Panahi [b,c], S. Kaya [b,c], T. Brinck [g], Y. Sassa [d], F.O.L. Johansson [e], J. Weissenrieder [a,*]

[a] Materials and Nano Physics, School of Engineering Sciences, KTH Royal Institute of Technology, SE-100 44 Stockholm, Sweden
[b] Koç University Tüpraş Energy Center (KUTEM), 34450 Istanbul, Turkey
[c] Department of Chemistry, Koç University, 34450 Istanbul, Turkey
[d] Department of Physics, Chalmers University of Technology, SE-41296 Göteborg, Sweden
[e] Division of X-ray Photon Science, Department of Physics and Astronomy, Uppsala University, SE-751 20 Uppsala, Sweden
[f] Department of Physics, AlbaNova University Center, Stockholm University, SE-106 91 Stockholm, Sweden
[g] Applied Physical Chemistry, Department of Chemistry, School of Engineering Sciences in Chemistry, Biotechnology and Health, KTH Royal Institute of Technology, SE-100 44 Stockholm, Sweden

ARTICLE INFO

Article history:
Received 4 May 2021
Revised 23 July 2021
Accepted 7 August 2021
Available online 13 August 2021

Keywords:
Heterogeneous catalysis
Acetic acid
Ketene
Scanning tunneling microscopy
X-ray photoelectron spectroscopy
Density functional theory

ABSTRACT

Ketene, a versatile reagent in production of fine and specialty chemicals, is produced from acetic acid. We investigate the synthesis of ketene from acetic acid over the (3,0;1,1) surface of $Cu_2O(100)$ through analysis of the adsorption and desorption characteristics of formic and acetic acids. The results allow us to establish a reaction mechanism for ketene formation. Observations from x-ray photoelectron spectroscopy (XPS), scanning tunneling microscopy, and temperature programmed desorption (TPD), supported by a comparison with formic acid results, suggest that acetic acid reacts with Cu_2O through deprotonation to form acetate species coordinated to copper sites and hydroxylation of nearby surface oxygen sites. For formic acid the decomposition of adsorbed formate species results in desorption of CO_2 and CO while, for acetic acid, high yields of ketene are observed at temperature >500 K. Modeling by density functional theory (DFT) confirms the strong interaction of acetic acid with the (3,0;1,1) surface and the spontaneous dissociation into adsorbed acetate and hydrogen atom species, the latter forming an OH-group. In an identified reaction intermediate ketene binds via all C and O atoms to Cu surface sites, in agreement with interpretations from XPS. In the vicinity of the adsorbate the surface experiences a local reorganization into a $c(2 \times 2)$ reconstruction. The total computed energy barrier for ketene formation is 1.81 eV in good agreement with the 1.74 eV obtained from TPD analysis. Our experimental observations and mechanistic DFT studies suggests that Cu_2O can operate as an efficient catalyst for the green generation of ketene from acetic acid.

© 2021 The Author(s). Published by Elsevier Inc. This is an open access article under the CC BY license (http://creativecommons.org/licenses/by/4.0/).

1. Introduction

The chemical flexibility of Cu_2O, that allows for facile storage or release of oxygen atoms, has rendered reactions over its surface a topic of great interest for heterogeneous catalysis (e.g. water-splitting [1,2], oxidation [3,4], dehydrogenation [5], photochemical CO_2 reduction reactions [6]). A particularly interesting subset of oxidation reactions involves the adsorption and decomposition of organic acids such as formic (HCOOH) and acetic (CH_3COOH) acids. Oxidation reactions occurring on copper surfaces in the presence of these acids and water are among the most important promoters for indoor atmospheric corrosion of electronic devices [7]. Reactions with acetic acid is however not limited to undesired degradation of materials, the decomposition of acetic acid on Cu(110) surfaces may result in the production of ketene (ethenone, H_2CCO) [8]. Ketene is produced on large scale in the production of acetic anhydride which in turn is a reaction intermediate for several important organic compounds (e.g. aspirin, coatings, pesticides, and preparation of cellulose acetates) [9]. Industrial production of ketene often proceeds through thermal pyrolysis of acetic acid or acetone by passing reactant vapors through heated pipes or nearby electrically heated metal wires at 1010–1030 K [10].

Peytral was first to propose a mechanism for the decomposition of acetic acid after analyzing the products from acetic acid decomposition in a platinum tube heated to 1400 K. He postulated three

* Corresponding author.
E-mail address: jonas@kth.se (J. Weissenrieder).

https://doi.org/10.1016/j.jcat.2021.08.022
0021-9517/© 2021 The Author(s). Published by Elsevier Inc.
This is an open access article under the CC BY license (http://creativecommons.org/licenses/by/4.0/).

reaction paths resulting in production of i) water and acetic anhydride, ii) methane and carbon dioxide, iii) formaldehyde, carbon monoxide and ethylene [11]. The inclusion of ketene into the mechanism was later suggested by Hurd and Martin from analysis of acetic acid pyrolysis in quartz tubes at 1020 K [12].

Thermal decomposition of acetic acid has recently been investigated over a wide variety of surfaces, e.g. silica, CeO_2(100), CeO_2(111), UO_2(111), TiO_2(100) and (110), $LaSrMnO_3$(100), and Fe_3O_4 [13–19]. Several reaction pathways and products have been observed. Ketene has been identified as a reaction product in the temperature range from 500 K to 700 K with yields dependent on chemical nature, composition, and structure of the surface [13–19]. Among these surfaces, acetic acid adsorption and decomposition have been investigated on TiO_2 surfaces, both from an experimental and theoretical point of view, and can be easily compared to the results obtained from Cu_2O surfaces [17,20–24]. Kim et al. [17] showed the importance of surface structure and composition for the reaction mechanism over TiO_2(001), where oxidized surfaces containing exclusively Ti^{4+} cations favors the formation of volatile organic products (such as ketene and acetone) whereas oxygen deficient surfaces favor CO production and carbon deposition on the surface. The same study also compared two surface structures, on a {011}-faceted surface acetates was found to decompose into ketene while on a {114}-faceted surface acetone was the major reaction product. On Cu(110), adsorption and thermal desorption of acetic acid have been studied by Bowker et al. [8], reporting desorption of carbon dioxide, acetic acid, and a significant amount of ketene. The suggested reaction path involves a high temperature acetic anhydride reaction intermediate bonded to the surface through both carboxylic functions.

In this paper we describe the detailed reaction mechanism for the conversion of acetic acid into ketene on Cu_2O(100). To accomplish this goal, we have used a combination of experimental techniques such as scanning tunneling microscopy (STM), temperature programmed desorption (TPD), x-ray photoelectron spectroscopy (XPS), together with modelling by density functional theory (DFT). Although the conversion of acetic acid into ketene over the Cu_2O(100) surface is the main focus of this paper, the study of formic acid chemisorption and decomposition turned out to be crucial to the understanding of the XPS and TPD results for acetic acid. First, we describe the adsorption of both molecules on the surface as investigated by STM and XPS, the deprotonation of both acids to form adsorbed formate [25–28] ($HCOO^-$) and acetate (CH_3COO^-) species (identified in the text by respectively formate* and acetate*), and the release of a hydrogen atom from the molecules. Then, we followed the thermal desorption of the adsorbed species by XPS and TPD. The decomposition of the formate* species leads to the desorption of CO_2 and CO, as confirmed by TPD, while high yields of ketene are observed in the case of acetic acid (at T > 500 K). Ketene observation by TPD is correlated with fingerprint XPS features that allowed us to suggest a reaction intermediate consisting of a ketene* molecule bonded via all C and O atoms to the surface. DFT studies confirmed the existence of the intermediate and allowed us to present a detailed mechanism for ketene formation suggesting that Cu_2O can operate as an efficient catalyst for the green generation of ketene from CH_3COOH.

2. Experimental section

The Cu_2O(100) single crystal used in this study is manufactured from a natural crystal acquired from the Surface Preparation Laboratory, the Netherlands. The cleaning procedure of the crystal consists of cycles of argon ion sputtering (0.5 kV, 20 min) followed by annealing in in oxygen gas (at 770 K, $P_{O2} = 3 \times 10^{-6}$ mbar) and in ultrahigh vacuum (at 910 K) [29,30]. The crystal cleanness in the low energy electron diffraction (LEED) and STM studies was confirmed by the sharpness of the LEED diffraction spots and by STM imaging exhibiting large and flat terraces. Fig. 1 presents XPS and STM analysis of the clean surface. No metallic copper or CuO were observed in the Cu LMM Auger (Fig. 1c) or in the Cu 2p (Fig. 1d) spectra. The STM-study was carried out using an Omicron VT-STM operated in constant current imaging mode with electrochemically etched tungsten tips. The STM-chamber is attached to a preparation chamber equipped with an ion sputter gun, leak-valves for introduction of gases, facilities for annealing the sample, and a LEED-apparatus. The base pressures in both the preparation chamber and the STM chamber were low 10^{-10} mbar. Commercial formic and acetic acid were used for these experiments (Sigma-Aldrich, purity > 99.5%). Acids were stored in glass vials and purified by several freeze-pumpthaw cycles before introduction to the analysis chamber via a leak valve.

2.1. XPS details

The XPS measurements were carried out at the UHV-XPS endstation at the PEARL beamline of the Swiss Light Source (Paul Scherrer Institute, Villigen, Switzerland) using a Scienta EW 4000 analyzer [31]. Sample preparation was conducted in a dedicated preparation chamber equipped with facilities for argon ion sputtering, sample annealing, and high precision leak valves [31]. All XPS binding energies were referenced to the Fermi level measured at a tantalum foil in direct electrical contact with the sample. After a Shirley-type background subtraction, spectra were fitted with Voigt (Gaussian–Lorentzian) functions. The width of the Lorentzian function was set at 0.35 eV.

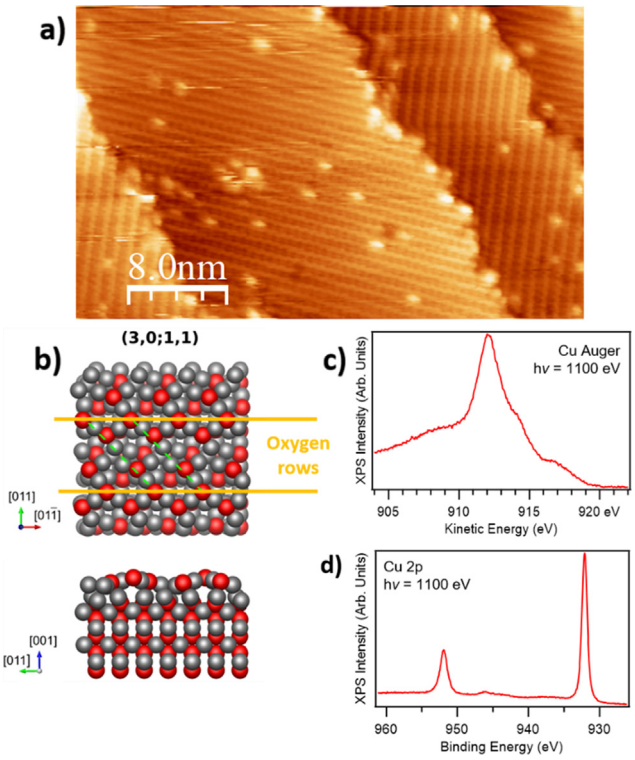

Fig. 1. Analysis of the clean Cu_2O(100) surface. a) STM image (STM scanning parameters: 3.0 V, 0.12 nA) b) surface structure model (yellow lines indicate the row observed in the STM image) c) Cu LMM Auger, and d) Cu 2p spectra (hν = 1100 eV). (For interpretation of the references to colour in this figure legend, the reader is referred to the web version of this article.)

2.2. TPD details

TPD measurements were performed in a UHV system equipped with a Specs ErLEED 100 optics, a Hidden HAL 201 RC quadrupole mass spectrometer, and crystal cleaning tools. The base pressure was better than 4×10^{-10} mbar. A K-type thermocouple placed between the Cu_2O crystal and a tantalum plate holder was used to measure the crystal temperature. Heating was performed resistively, by running direct current through tantalum wires clamping the tantalum plate holder onto the sample manipulator rod. The crystal temperature is feedback-controlled within 100–1000 K. The mass spectrometer utilized to detect desorption products was mounted in a differentially pumped housing with an 8 mm OD opening to the vacuum side. The tip of this housing was placed 0.5 mm above the crystal surface to minimize the detection of the desorbing molecules outside the surface. The heating rate in the TPD analysis was 3 K/s.

2.3. Computational details

The surface modeling was conducted by periodic and spin-polarized DFT calculations with the Vienna Ab initio Simulation Package (VASP) [32]. The PBE exchange-correlation functional was employed in combination with Hubbard corrections using a $U - j$ value of 3.6 eV as well as D3 dispersion corrections [33–36]. The valence states (Cu: $3d^{10}4s^1$; O: $2s^22p^4$; C: $2s^22p^2$; H:$1s^1$) were expanded on a plane-wave basis set with a cut-off of 400 eV, whereas the electronic core states were represented by standard PBE PAW potentials [37,38]. A Γ-centered $2 \times 2 \times 1$ k-point mesh was used for the sampling of the Brillouin zone using the tetrahedron method with Blöch corrections [39]. The Cu_2O (100) surface was modeled by the (3,0;1,1) and c(2×2) reconstruction structures of Soldemo et al. [29] using enlarged *p* (3×3) supercells. A six Cu_2O-layer thick asymmetric slab was used with a vacuum distance of 20 Å. The top two layers were allowed to relax. The forces and electronic energy were converged to 0.03 eV/Å and 10^{-6} eV, respectively.

O and C 1s XPS core level shifts (CLS) were computed using the final state approximation, following the procedures of Soldemo et al. [29]. This is for an atom (O or C) surface state i, the CLS = E_i – E_{ref}, where the reference state (ref. [40,41]) can be another surface atom or a bulk atom.

CCSD(T)/aug-cc-pvtz single-point energy calculations for the gas-phase reactions were carried out in the G16 program suit (version C.01) [42]. The structures were first optimized at the PBE/6-311+G(2d,2p) level. Vibrational analysis for the thermochemical corrections was performed at the PBE/6-311+G(2d,2p) level, employing the ideal gas, rigid rotator, and harmonic oscillator assumptions.

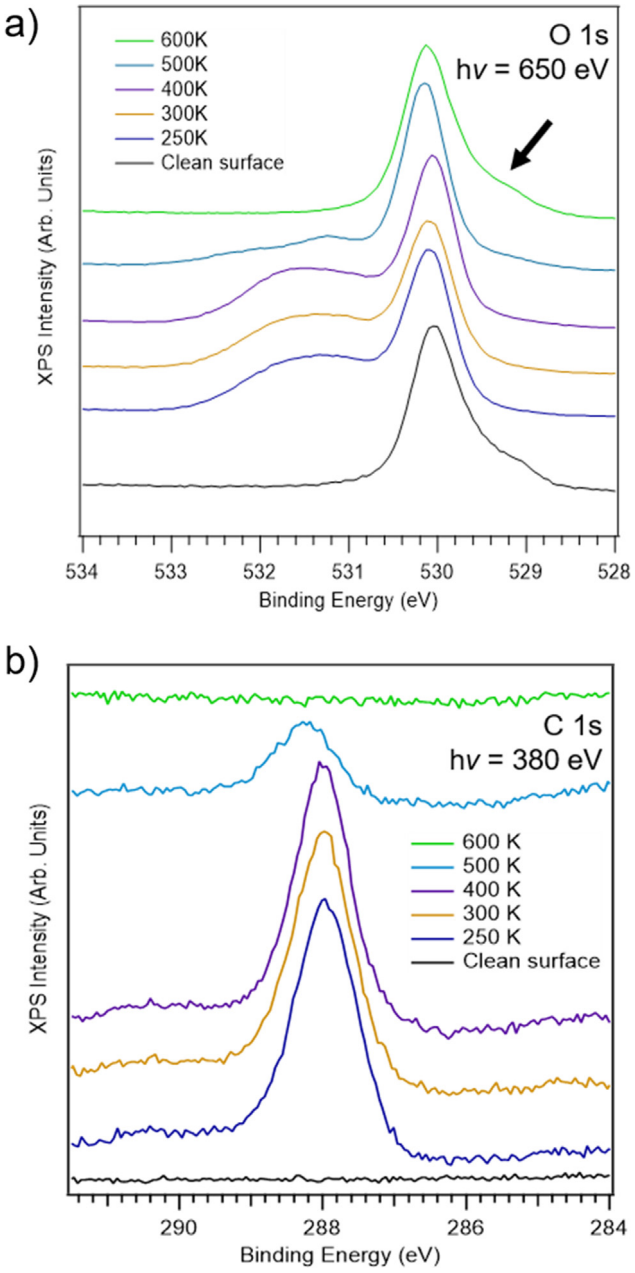

Fig. 2. a) O 1s and b) C 1s XPS spectra at increasing temperature after exposure of the clean Cu_2O(100) surface to formic acid at 120 K (1×10^{-8} mbar, 5 min, 2.25 L). Spectra were collected using a photon energy of 650 eV (O 1s) and 380 eV (C 1s). The black arrow in a) indicates the position of the surface peak associated with the reconstruction of the clean surface.

3. Results

The clean Cu_2O(100) surface was first exposed to 1×10^{-8} mbar of formic acid for 5 min at 120 K (or 2.25 Langmuir, L) in the preparation chamber and, after transfer to the analysis chamber, analyzed by XPS (during transfer the sample temperature may have increased to a maximum 180 K). Fig. 2a presents O 1s spectra as a function of annealing temperature, fitted spectra collected at 400 and 500 K are presented in supporting information Fig. S1. The main peak at 530.2 eV represents lattice oxygen atoms positioned in the bulk of the crystal. A large shoulder can be observed at higher binding energy (extending from 530.7 to 532 eV). This shoulder contains at least two components, one corresponding to hydroxyl groups on the Cu_2O surface (+1.1 eV from the main O 1s peak as reported by Stenlid et al. and Tissot et al. [43,44]) and at least one to formate species (with a peak position between +1.8 to +2.1 eV in our fit in Fig. S1). However, the broad structure of the shoulder renders fitting parameters and relative coverage somewhat uncertain. Yao et al. has, on an oxygen pre-covered Cu (110) surface, observed two components in the O 1s spectrum, at 530.4 and 531.8 eV, associated with different adsorption configurations of formate* [45], suggesting that the component at +1.1 eV is not exclusively composed of surface hydroxyl groups. On the other hand, on the TiO_2(110) surface, Chambers et al. observed formate species at a binding energy of 532. 1 eV (+1.7 eV from the TiO_2 oxygen component) [27]. The adsorbate shoulder at high binding energy disappears at 600 K. Simultaneously, we observe a low binding energy peak at ~529 eV (black

arrow in Fig. 2a) associated with the reconstruction of the clean $Cu_2O(100)$ surface [29].

In the C 1s spectra, presented in Fig. 2b, a lone peak is observed at 287.8 eV corresponding to the carbon atom of formate* species on the surface, confirming deprotonation of the acid [46]. The peak disappears between 500 K and 600 K, reflecting the desorption of surface species. At 500 K both C 1s and O 1s peaks are shifted by ~0.2 eV. This shift is interpreted as a result from band bending due to a modification of the surface during the desorption process. At 600 K the surface is free of carbon species in agreement with the recovery of a clean $Cu_2O(100)$ surface as already observed in O 1s. The XPS observations points to a mechanism where deprotonation of the formic acid results in formation of formate* species and hydroxyls groups, the latter through coordination of an adsorbed hydrogen (H*) to a surface oxygen atom.

Formic acid adsorption was also studied on a pre-hydroxylated $Cu_2O(100)$ surface obtained by exposing the clean surface to water at 120 K at a pressure of 5×10^{-8} mbar for 5 min (11 L) as presented in Fig. S2 of the Supporting Information. Pre-hydroxylated surfaces showed similar surface products and desorption behavior, indicating that hydroxylation does not play a major role in the reaction mechanism.

The results from formic acid was then compared with acetic acid adsorption on the clean $Cu_2O(100)$ surface. The surface was exposed to 2.5×10^{-8} mbar of acetic acid for 2.5 min at 120 K (2.25 L). Fig. 3a presents the evolution in the O 1s spectra with temperature. Oxygen atoms residing at lattice sites in the bulk of the crystal are found at 530.2 eV and a large adsorbate shoulder is observed at higher binding energy, between 530.7 and 532 eV. This shoulder disappears at a temperature of 700 K. A comparison of the formic and acetic acid adsorption results shows some differences. The high binding energy shoulder for acetic acid adsorption at 500 K (blue curve) is less intense than at 400 K and does not exhibit a well-defined two-component structure as was the case for formic acid. In the case of formic acid the adsorbate shoulder at high binding energy disappears at 600 K, while for acetic acid at this temperature a single peak is observed at +1.77 eV (indicated by a green arrow in Fig. 3a). This peak is well separated from the peak of oxygen atoms at lattice sites in the bulk of the crystal (curve fitting in supporting information Fig. S3). Taken together, the observations suggest a similar adsorption mechanism as previously discussed for formic acid. Adsorption of acetic acid will result in the formation of acetate* species and OH* groups through dissociation of the OH group of acetic acid. During annealing we observe a shift of the main O 1s peak corresponding to oxygen atoms at bulk lattice positions. A maximum shift (~0.2 eV) is obtained at 300–400 K (A similar shift is observed for the Cu 2p as presented in SI Fig. S4). At further increasing temperature the peak shifts back to the position of the clean surface (after annealing to 700 K). This shift is also observed for the other core-levels and is associated with a band bending at the surface. The observed band bending is similar for formic and acetic adsorption and is probably related to the desorption of water observed in TPD at 200–350 K or to a reordering of adsorbates on the surface. At about 600 K we begin to observe the reappearance of the low binding energy fingerprint peak at ~529 eV, associated with the reconstruction of the clean surface (black arrows in Fig. 3a) [29].

Fig. 3b presents the corresponding C 1s spectra as a function of temperature. At 400 K and below the spectra show two main peaks. The peak at 287.9 eV is assigned to the carbon atom of the carboxyl group in acetate* species. This fits in well with the position observed for the carboxyl group of formate* (287.8 eV). The second peak, at 284.7 eV, is attributed to the carbon atom of the methyl group.

The asymmetry of the high energy C 1s peak at 120 K is due to the presence of a component at 288.7 eV related to carboxyl groups

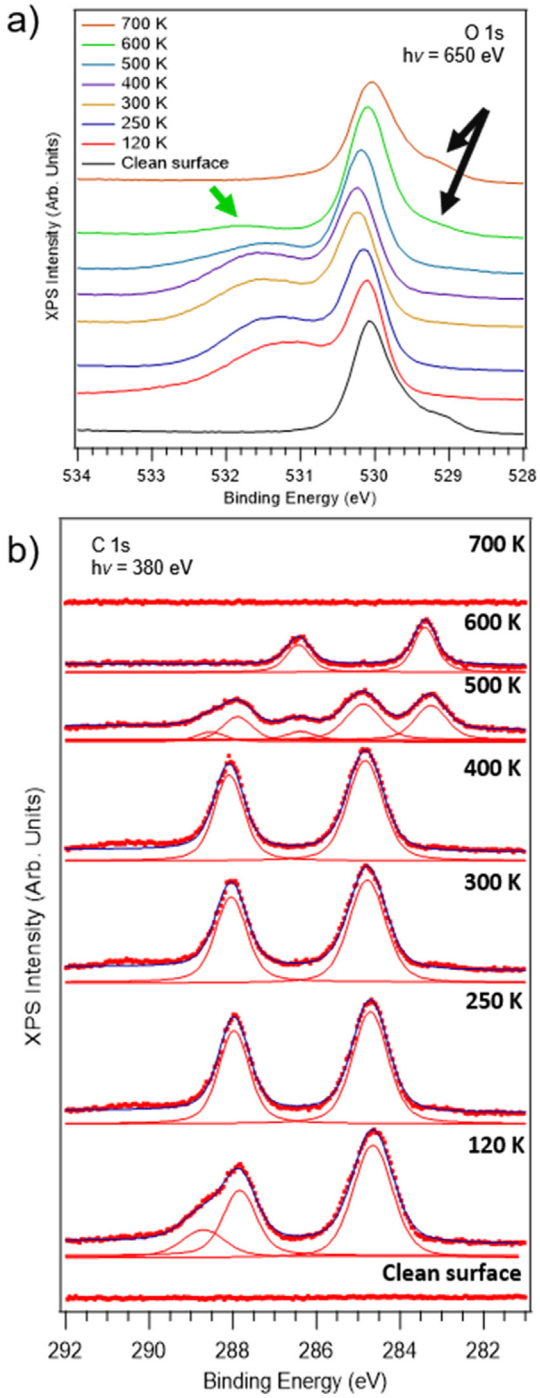

Fig. 3. XPS spectra a) O 1s and b) C 1s including curve fits of the clean $Cu_2O(100)$ surface exposed to acetic acid at 120 K (2.5×10^{-8} mbar, 2.5 min, 2.25 L). The spectra were collected at photon energies of 650 eV (O 1s) and 380 eV (C 1s). The arrows in a) indicate the position of the peak associated with the clean surface reconstruction (black) and the separated peak observed at +1.77 eV at 600 K (green). (For interpretation of the references to colour in this figure legend, the reader is referred to the web version of this article.)

in intact acetic acid molecules physisorbed through H-bonding to the surface (confirmed by spectra recorded after exposure to a large dose of acid at low temperature that formed physisorbed acetic acid layers). A peak corresponding to the methyl group of the physisorbed molecules may also be detected in the line shape and intensity of the low energy component. The binding energy shift of the physisorbed methyl group compared to the methyl

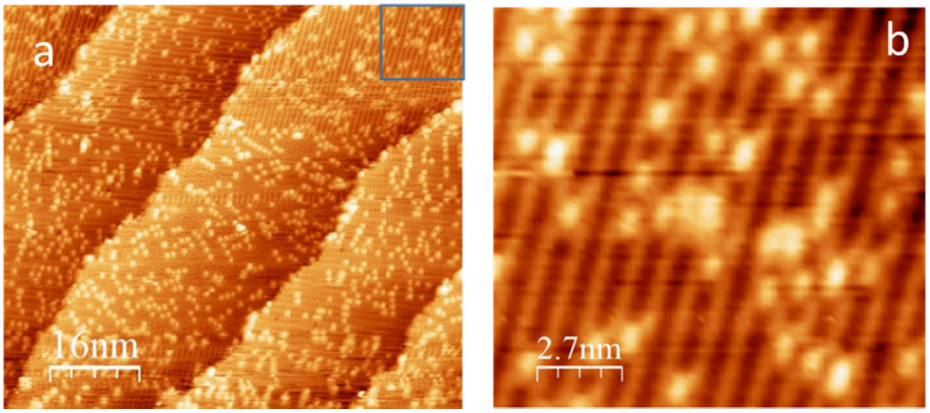

Fig. 4. STM images of the $Cu_2O(100)$ surface after a) exposure to acetic acid at 4×10^{-9} mbar for ~10 s (0.03 L) at 300 K (STM scanning parameters: 3.0 V, 0.12 nA). b) shows an enlarged view of the area indicated by the rectangle in a).

group of the adsorbed molecule is too small to allow it to be resolved in the C 1s spectrum. Similar spectral features were observed by Dover et al. after exposure of $TiO_2(110)$ to acetic acid at high pressures (>10^{-5} mbar). Two peaks associated to acetic acid were detected their study, but only in the high binding energy component (~290 eV) could a shoulder be resolved that was assigned to physiosorbed species [23].

A careful analysis of the peak intensities shows that the methyl group peak corresponds to 57% of the total C 1s intensity and the combination of the carboxyl groups peaks at 287.8 and 288.7 eV to 43%. A 60:40 intensity ratio between the CH_3 and COO peaks has previously been reported for acetic acid adsorption on several surfaces and is not due to X-ray beam damage but an effect from screening of the methyl group pointing outwards of the surface [47,48].

Desorption of physisorbed species takes place at temperatures below 250 K as indicated by the disappearance of the 288.7 eV shoulder in the C 1s spectra. The ratio between the two main C 1s peaks remains 43%:57% also after desorption of the physisorbed layer. This implies that the desorption of the physisorbed acetic acid leaves the adsorbate structure intact. Further changes to the C 1s spectrum are observed at 500 K. The carboxyl peak at 287.9 (23%) and the methyl peak 284.9 eV (33%) that is associated with acetate* species are still observed. The observation of a shoulder at 288.8 eV (6%) at 500 K can not be attributed to physisorbed acetic acid. Carbonate and $CO_2^{\delta-}$ species were previously observed by Deng et al. at binding energies 289.3 eV and 288.7 eV for CO_2 adsorption on a polycrystalline Cu foil in the presence of water [49]. In our case, it is difficult to discriminate between a carbonate species adsorbed on a surface Cu atom and a $CO_2^{\delta-}$ adsorbed on a surface oxygen atom. Interestingly, at 500 K we observe two additional peaks at 286.6 eV and at 283.3 eV. These two peaks are the only remaining after annealing to 600 K, with peak positions and relative intensities of 286.5 eV (40%) and 283.3 eV (60%). The assignment of these peaks is not trivial. The peak at 286.5 eV must be associated with a carbon atom linked to an oxygen atom. The peak should therefore be associated with the observed high binding energy feature in the O 1s spectrum recorded after annealing to 600 K. The O 1s curve fit presented in Fig. S3 (Supporting Information) shows a peak with a binding energy shift of +1.77 eV with respect to the oxygen atoms at Cu_2O lattice sites. The assignment of the 286.5 eV and 283.3 eV peaks will be discussed in further detail under the Discussion section.

At 500 K we observe changes to the Cu LMM Auger spectra (Fig. S4b). A weak shoulder appears at a kinetic energy position corresponding to metallic copper. No apparent change was observed in the Cu 2p spectrum (Fig. S4a). This is not surprising since differentiating Cu_2O from Cu is known to be difficult in Cu 2p spectra. The formation of metallic Cu can be explained by a water formation reaction, through abstraction of an surface oxygen atom, and subsequent desorption [44]. The metallic copper component disappears at 700 K, tentatively through diffusion of metallic Cu into the bulk of the crystal.

The influence of pressure and pre-hydroxylation on the interaction of acetic acid with $Cu_2O(100)$ was studied by exposure to acetic acid at 1×10^{-2} mbar for 2 min at 300 K and by first dosing the clean $Cu_2O(100)$ surface with H_2O at 120 K (5×10^{-8} mbar for 5 min at 120 K, 11 L) followed by acetic acid exposure at 5×10^{-8}-mbar for 5 min at 120 K (11 L). Similar to what was previously observed for formic acid adsorption, neither the pressure of acetic acid in the exposure step nor its adsorption on a pre-hydroxylated surface resulted in any significant changes in the XPS results suggesting that pressure and preexisting surface OH groups do not influence the reaction mechanism (see Figs. S5 and S6 in the Supporting Information).

STM analysis was performed in order to study potential changes in surface morphology of the $Cu_2O(100)$ surface following exposure to acetic acid and during subsequent annealing steps. Fig. 4 presents STM images of the surface after exposure to 4×10^{-9} mbar during ~10 s (0.03 L) at 300 K. Elongated bright spots are observed at positions in between the atomic oxygen rows of the (3,0;1,1) surface reconstruction. From our previously described XPS results we expect acetate* and hydroxyl* groups at the surface at this temperature. The protrusions are interpreted as a combination of acetate* and a hydroxyl* groups, where the hydroxyl* is formed by deprotonation of the acid and OH formation at a nearby surface oxygen site.

Hydroxyl groups cannot be observed independently from the acetate species in the STM analysis. From our previous study of atomic hydrogen adsorption on $Cu_2O(100)$, we know that among the three available surface oxygen sites on the surface (one fully exposed in the surface rows and two in between the atomic rows of the surface layer), the formation of hydroxyl groups occurs at a valley site. Therefore, the hydroxyl group will be positioned close to the acetate species in the valley between the rows resulting in one elongated protrusion in the STM analysis.

Fig. 5 presents the evolution of this surface as a function of annealing temperature. At 480 K (Fig. 5b) we observe formation of depressions in the surface (as dark defects) that can be coupled to the desorption process. Except for a few bright protrusions attributed to remaining organic species and metallic copper (as suggested by XPS) the structure of the clean reconstructed surface is almost completely recovered after annealing to 560 K. As comparison an STM image of the clean surface is presented in Support-

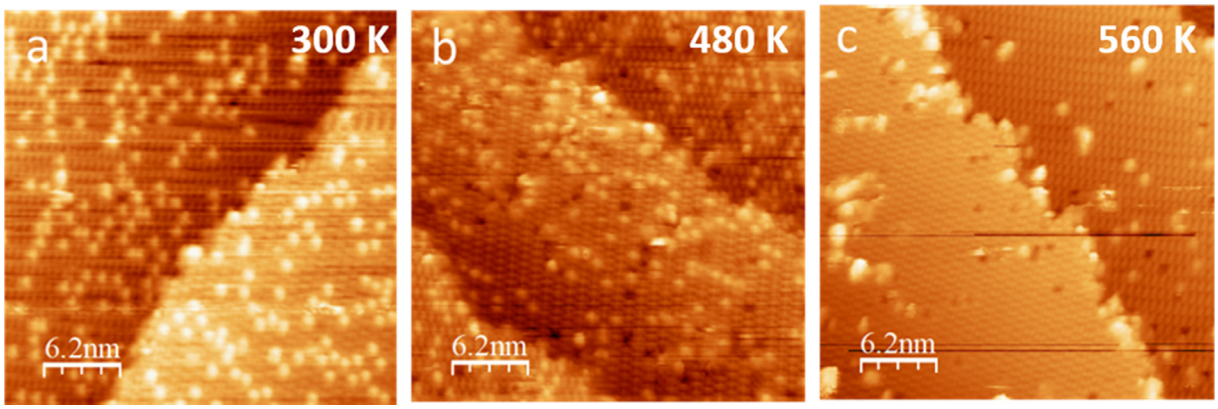

Fig. 5. STM images of the $Cu_2O(100)$ surface a) after exposure to a low dose of acetic acid (4×10^{-9} mbar for 10 s, ~0.03 L) at 300 K (STM scanning parameters: 3.0 V, 0.12 nA); b) after annealing in UHV to 480 K (2.9 V, 0.16 nA) and c) following annealing to 560 K (3.5 V 0.22 nA).

ing Information Fig. S7a. After desorption of surface species, the terrace edges exhibit more irregular shapes compared to the clean initial surface (an example of a surface dosed by 0.08 L and annealed to 590 K is given in Fig. S7 of the Supporting Information).

The $Cu_2O(100)$ surface was also studied after a higher dose of acetic acid (10^{-2} mbar for 2 min at 300 K). The evolution of the surface structure and morphology as a function of annealing temperature is presented in Supporting Information Fig. S8. At 300 K the surface is completely covered by protrusions. The protrusions are assigned to acetate* and OH* species. In a comparison of Figures S8a (300 K), b (480 K), and c (560 K) we find the surface morphology mostly unaffected by annealing even to 560 K. This finding is in agreement with the previously presented XPS results, confirming that the adsorbates derived from acetic acid remains on the surface below 600 K. A carful inspection of the images collected at different temperatures uncovers a difference in the density and size of clusters on the surface. Clusters with increasing size and prevalence with temperature are attributed to metallic copper clusters. This result brings us back to the Cu LMM Auger spectra presented in Fig. S4b, which show a significant metallic contribution in the temperature range 500–600 K. Formation of similar metallic copper clusters has previously been observed on the $Cu_2O(100)$ during reduction upon the exposure to atomic hydrogen [44]. This shows that clusters are favorable structures for metallic copper on this surface. The desorption of surface species is complete after annealing to 650 K and the characteristic rows of the reconstructed clean surface can once more be observed. The absence of copper clusters in Fig. S8d suggests, in line with the Cu LMM analysis, that copper

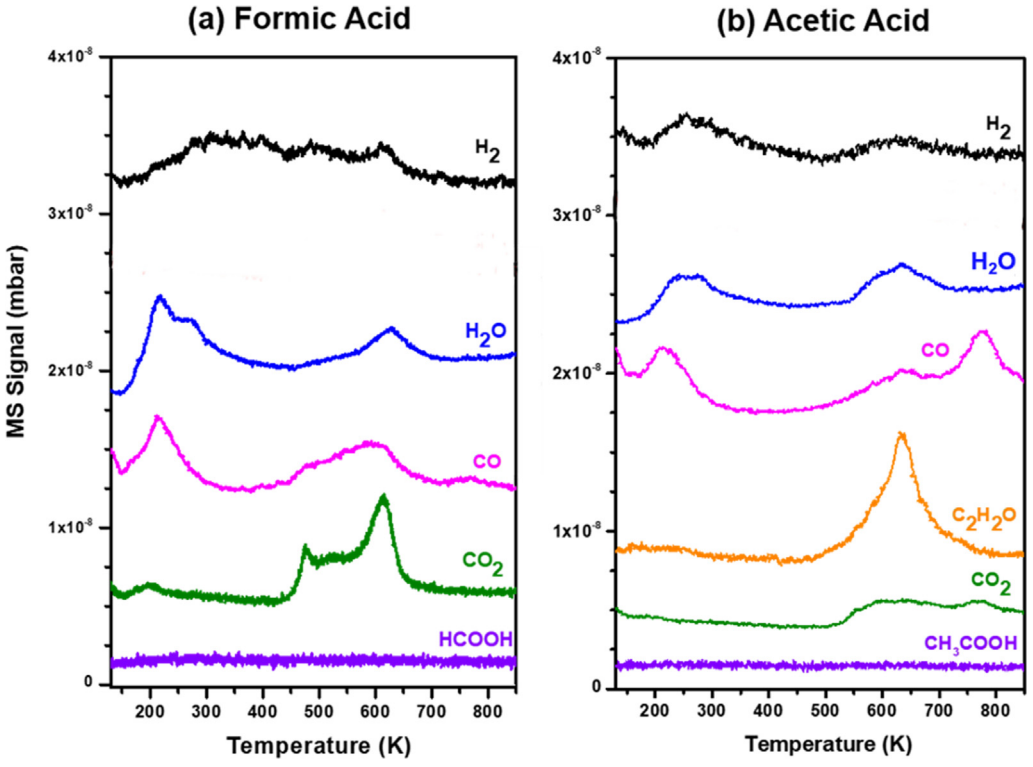

Fig. 6. TPD spectra for relevant products following exposure at 105 K of the clean $Cu_2O(100)$ surface to 3 L (a) formic acid and (b) acetic acid (3 L). The spectra are offset for clarity. The masses followed in a) are: 2 amu (H_2), 18 amu (H_2O), 28 amu (CO), 44 amu (CO_2), and 46 amu (HCOOH). The masses followed in b) are: 2 amu (H_2), 18 amu (H_2O), 28 amu (CO), 42 amu (C_2H_2O), 44 amu (CO_2), and 60 amu (CH_3COOH).

diffuse into the bulk of the crystal. The low coverage of bright protrusions observed in Fig. S8d is attributed to oxygen vacancies, as described earlier [30].

Further understanding of the chemical process taking place on the Cu_2O surface can be obtained by analyzing the TPD products resulting from the dosage of formic and acetic acid. TPD experiments for both acids are presented in Fig. 6, whereas TPD spectra for different acid coverage can be found in Figs. S9 and S10 in the Supporting Information. TPD at low temperature shows mainly physisorbed species present on the surface, such as CO and water coming from the gas line or the background pressure of the chamber. From 500 K, decomposition of the formate* into carbon dioxide/monoxide and water starts as already observed by Poulston et al. on bulk copper oxides powders [50]. In the case of $(m/e)^+ = 44$ amu associated with CO_2 desorption, two decomposition peaks appear at 480 K and 600 K that can be associated to two coverage-dependent formate* adsorption modes, possibly a monodentate and bidentate species, with the bidentate species being more strongly bonded to the surface and desorbing at a higher temperature. Similar desorption temperatures were observed for copper surfaces exposed to formic acid: e.g. on Cu(1 1 0) a CO_2 desorption peak was found at 480 K, but on oxygen precovered Cu (1 1 0) a shoulder appears at a lower temperature of 430 K [51]. Two peaks are found on CuO bulk powder, at 430 K and 545 K. Similarly on Cu_2O bulk powder peaks are found at 375 K and 485 K [50]. In the same temperature range, water and carbon monoxide desorption can also be observed. Water desorption can be explained by recombination of OH* and H* atoms with the oxygen atom being initially a surface atom or a result of the scissoring of a C—OH bond of formate* leading to H_2O and CO.

For acetic acid, at T > 500 K, water and CO are observed as well as a small amount of CO_2. The CO_2 desorption peak covers a large temperatures window (500–700 K) and do not exhibit the two well-defined peaks found at 480 and 600 K in the case of formic acid. It is therefore difficult from these results to conclude if the adsorption configuration of acetate* species is monodentate or bidentate. It is also difficult to identify which copper site(s) is (are) involved in the binding and desorption process. The wide band observed for CO_2 desorption (instead of two clear peaks) suggests several adsorption modes. However, the detection of CO_2 is in agreement with the carbonate/$CO_2^{\delta-}$ species observed by XPS (CO and CO_2 desorbing above 725 K are attributed to the reaction of adventitious carbon with the surface oxygen).

The main difference between the TPD of both acids is the strong peak, mass at $(m/e)^+ = 42$ amu, with a maximum at 630 K for acetic acid. This mass is related to ketene. The identification is supported by observations by Bowker et al. for acetic acid adsorption on Cu (1 1 0) [8]. The observation of ketene among desorption molecules is interesting and send us back to the XPS results in Fig. 3. Ketene desorption confirms that the C—C bond from the acetic acid skeleton remains largely unbroken on the surface.

4. Discussion

XPS and TPD observations suggest that low temperature adsorption of both formic and acetic acid results in formation of thick layers of physisorbed acid molecules. At the interface between Cu_2O and the acid layer, molecules react with the surface by deprotonation of the acid to form respectively formate* and acetate* species bonded to surface copper atom sites. The dissociation of the inner layer releases hydrogen atoms that bind to either nearby surface oxygen or copper sites. The OH* signature in O 1s XPS spectra suggests the first option. However, the presence of Cu—H bond on the surface cannot be excluded spectroscopically. Physisorbed acid molecules have desorbed at 250 K leaving only chemisorbed species on the surface.

Between 400 and 700 K the surface species undergo further reactions, resulting in decomposition of formic and acetic acid. In the case of formic acid, TPD confirms the decomposition through observation of CO_2, CO, H_2O, and traces of H_2. The decomposition corresponds to the following main reactions:

$$HCOOH \rightarrow CO_2 + H_2 \quad (1)$$

$$HCOOH \rightarrow CO + H_2O \quad (2)$$

For acetic acid, decomposition into CO and CO_2 (reactions (3) and (4)) is also observed by TPD, however, they constitute minor reaction pathways. The main reaction path for acetic acid decomposition at high temperature on Cu_2O(1 0 0) leads to the desorption of ketene and water (reaction (5)). The formation of ketene and water is consistent with observations on other surfaces such as CeO_2(1 0 0), CeO_2(1 1 1), UO_2(1 1 1), TiO_2(1 0 0), $LaSrMnO_3$(1 0 0) and Fe_3O_4 [13–17,19]; however, acetaldehyde and acetone are not observed here while they were on CeO_2 surfaces.

$$CH_3COOH \rightarrow CO_2 + CH_4 \quad (3)$$

$$CH_3COOH \rightarrow 2CO + 2H_2 \quad (4)$$

$$CH_3COOH \rightarrow CH_2{=}CH{=}O + H_2O \quad (5)$$

The low proportion of H_2 and absence of CH_4 in TPD is in contrast with what is expected from stoichiometry of reactions (4) and (3) and suggests that the above reactions are coupled to Cu_2O reduction via abstraction of surface oxygen atoms. This explains the relatively high H_2O, CO, and CO_2 TPD signals, at the expense of H_2 and CH_4.

In our previous study of atomic hydrogen adsorption on the clean Cu_2O(1 0 0), [44] the adsorption of H* on the surface resulted in a OH group located in the valley between the oxygen rows of the reconstructed surface. The main desorption pathway at elevated temperature was through H_2 desorption. However, the reaction involved migration of the OH to the Cu trimer site of the surface. In the case of acetic acid adsorption, the Cu trimer sites are already occupied by the acetate species. Therefore, H_2 desorption cannot follow a similar route. Instead, in agreement with TPD results, H_2O desorption is favored through a Mars-Van Krevelen mechanism. This was only a minority reaction path in the case of atomic hydrogen adsorption, but results in the formation of metallic Cu clusters on the surface as observed by STM [44]. In our current STM results we also observe copper clusters on the surface during acetic acid decomposition and the Cu LMM Auger spectrum exhibits a characteristic peak for metallic copper in the temperature range 500–600 K. It is interesting to note that no carbide species are observed at low BE energy in the C 1s spectra. The desorption of surface species is complete after annealing to 650 K and the characteristic surface reconstruction of the clean surface can be observed in STM.

Reaction (5) and the observation of ketene desorption is specific to acetic acid. Ketene formation has been reported by Wang et al. on TiO_2 surface [52] and by Bowker et al. in the case of acetic acid adsorption on Cu(1 1 0) [8]. Bowker et al. suggests formation of a high temperature anhydride acetate reaction intermediate bonded to the surface through both carboxylate functions. The existence of this intermediate is justified by the desorption of ketene and acetic acid, the major products of acetic anhydride decomposition. However, in the present study no acetic acid desorption is observed in TPD and it is difficult to rationalize the presence of a anhydride acetate reaction intermediate in the C 1s spectra at 500 and

600 K, where two carbon types of this intermediate are expected to appear at higher binding energies.

Reactions performed on metals described in the literature can be of help here. Ketene adsorption on Pt(1 1 1) [53] has a molecular adsorption intermediate that decomposes at 280 K and is bonded to the surface through both carbon atoms creating a four-member ring with two metal surface atoms been observed. The main TPD desorption products are ketene, CO, CH_4 and H_2 [53]. A similar structure on Cu_2O is schematically depicted in Fig. 7.

Information from XPS were used to validate this structure by the observed features in the C 1s spectrum at 500 K and 600 K (Fig. 3b). A carbon atom in the methylidene group (H_2C=) directly bonded to a surface copper atom can be expected to show up at a low binding energy in the C 1s spectrum due to the electropositive character of the metal compared to the carbon atom. This agrees with the peak observed at 283.3 eV. The carbon atom of a carboxyl group protruding out of the surface, with its double bond to the oxygen atom, is expected at a binding energy of ~287–288 eV. But since the carbon atom in the suggested intermediate coordinates to a surface copper atom it can be expected to appear at a lower binding energy. The binding energy can be expected to shift even lower if the oxygen atom of the intermediate also coordinates to Cu sites of the substrate. This is also in agreement with the peak at 286.5 eV observed Fig. 3b. In the suggested adsorption geometry, the reaction intermediate requires at least two copper atoms separated by ~150 pm. The Cu_2O(1 0 0) surface expose sites constituted of three copper atoms in between oxygen rows of the reconstruction, as further described in ref. [29]. These are appropriate sites for this type of intermediate. Furthermore, this is in agreement with STM observations, where bright protrusions due to acetic acid adsorbates are located in-between the oxygen rows at room temperature as well as at 500 K.

In order to bring further light upon the atomic scale details of the processes leading to the generation of ketene from acetic acid on Cu_2O(1 0 0), we model the reaction mechanism by DFT guided by the experimental information gathered by XPS, STM, and TPD. The overall gas-phase reaction of acetic acid leading to ketene and water (reaction (5)) has a standard reaction enthalpy, $\Delta H°_R$, of 1.48 eV (i.e., 143.5 kJ/mol) [54,55]. The Gibbs free energy of the reaction, ΔG_R, at 600 K is 1.03 eV at 1 bar partial pressures. However, at 10^{-10} bar partial pressure corresponding approximately to the experimental conditions reported herein, ΔG_R is exergonic at −0.80 eV (assuming ideal gases). The standard reaction enthalpy is well-reproduced computationally at the PBE-D3 +U GGA-DFT level ($\Delta H°_R$ = 1.43 eV), which is also in close agreement with our CCSD(T)//PBE-D3 calculations ($\Delta H°_R$ = 1.48 eV).

We now compare the reaction energy of ketene (ethenone) to structural isomers that could also correspond to the mass of $(m/e)^+$ = 42 amu observed in the TPD analysis. At the CCSD(T)//PBE-D3 (PBE-D3) level of theory, the $\Delta H°_R$ are 3.37 (3.44), 1.47 (1.65), and 4.25 (3.25) eV for oxirene, hydroxyacetylene, and formylmethylene, respectively (see Fig. S11 for structures) - i.e., less stable than ketene. This is in-line with previous findings and shows that ketene is the most stable isomer. It also demonstrates that ketene indeed is a likely product [56].

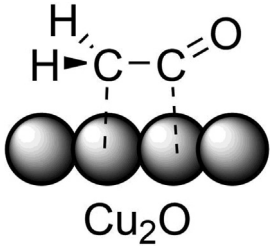

Fig. 7. Schematic illustration of reaction intermediate suggested from experimental observations.

The experimental results together with previous knowledge of the system provide guidance for the selection of a model system. It has previously been demonstrated that the employed preparation protocol for the Cu_2O(1 0 0) surface leads to a (3,0;1,1) surface reconstruction [29]. This is confirmed herein by results from STM, LEED, and the fingerprint shoulder peak at 0 to −1 eV towards lower energy with respect to the O 1s lattice peak in the XPS spectrum of the clean surface in Figs. 2 and 3. Upon interaction with chemisorbing species of the type ROH (R = H, CH_3, CH_3CH_2), as well as other adsorbates (e.g. H_2, CO, O_2,), we have in earlier work observed that the surface reconstruction is lifted [5,29,43,57,58]. This is accompanied by the dissociation of the adsorbate into RO* + H*. The resulting surface has a (1 × 1) or c(2 × 2) symmetry and a Cu-termination, with RO* and H* competing for the same type of Cu—Cu bridge adsorption sites. The atomic structures of the (3,0;1,1) and c(2 × 2) surfaces are shown in Fig. 8.

The formation of ketene from acetic acid is studied on both the (3,0;1,1) and c(2 × 2) model surfaces. We assume a coverage corresponding to one acetic acid molecule per (3,0;1,1) unit (i.e., 1/6 ML with respect to surface copper atoms, or 3.04×10^{-12} molecules per cm^2). Whereas the full data for this is enclosed in the Supporting Information, the following discussion will show the most favorable reaction path (see Fig. 9). We start off by showing the energetics at 0 K followed by a discussion of the thermal effects.

Acetic acid interacts strongly with the (3,0;1,1) surface, with an adsorption enthalpy of –1.05 eV. The molecule binds bidentate via both O atoms towards the Cu-trimer site in-between the (3,0;1,1) ridges that are seen in the STM images (e.g. Fig. 4 b). Our computational results suggest that acetic acid spontaneously dissociates to acetate* and H*, the latter forming an OH-group with a nearby surface oxygen atom as shown in Fig. 10, in agreement with the observation of only one protrusion for both acetate* and OH* in between rows in Fig. 4. This dissociated state is at −1.22 eV versus acetic acid in the gas-phase. Subsequent local reorganization of the surface to the c(2 × 2) is energetically beneficial, as this structure better accommodates the adsorbates. Part of the explanation comes from the enhanced flexibility of Cu in the c(2 × 2) surface where the Cu atoms can adapt to best satisfy the adsorbates' binding preferences. The stronger adsorption in this surface configuration overcomes the +0.72 eV/(3,0;1,1)-unit reconstruction energy of the surface, leaving the surface with acetate* and H* adsorbed at −1.52 eV versus the acetic acid gas-phase reference. A corresponding surface effect is also found upon adsorbing formic acid on the surface (see the Supporting Information). These are the expected structures for acetate and formate at low temperatures (<450–500 K), and low coverage. As the surface becomes crowded, other adsorption modes such as mono-dentate chemisorption and physisorption are possible.

We believe that the above adsorbate-induced surface reorganization is local and restricted to the vicinity of the adsorbate. This cannot be directly confirmed by STM since the reconstruction will only occur locally, under the adsorbate. At low coverage and at a distance from the adsorbate, the (3,0;1,1) reconstruction is kept generally intact. At higher coverage, our interpretation is supported by the loss of the finger-print peak for the (3,0;1,1) reconstruction in the O 1s XPS spectrum. Furthermore, irregularities observed at terrace edges by STM for annealing temperatures of 560–590 K after desorption of acetic acid decomposition products, (see supporting information Fig. S8) suggest a high mobility of copper atoms on the surface in the presence of chemisorbed acetic acid fragments.

At higher temperatures (>500 K), the significant barrier for a further reaction from this stable state can be overcome. As shown

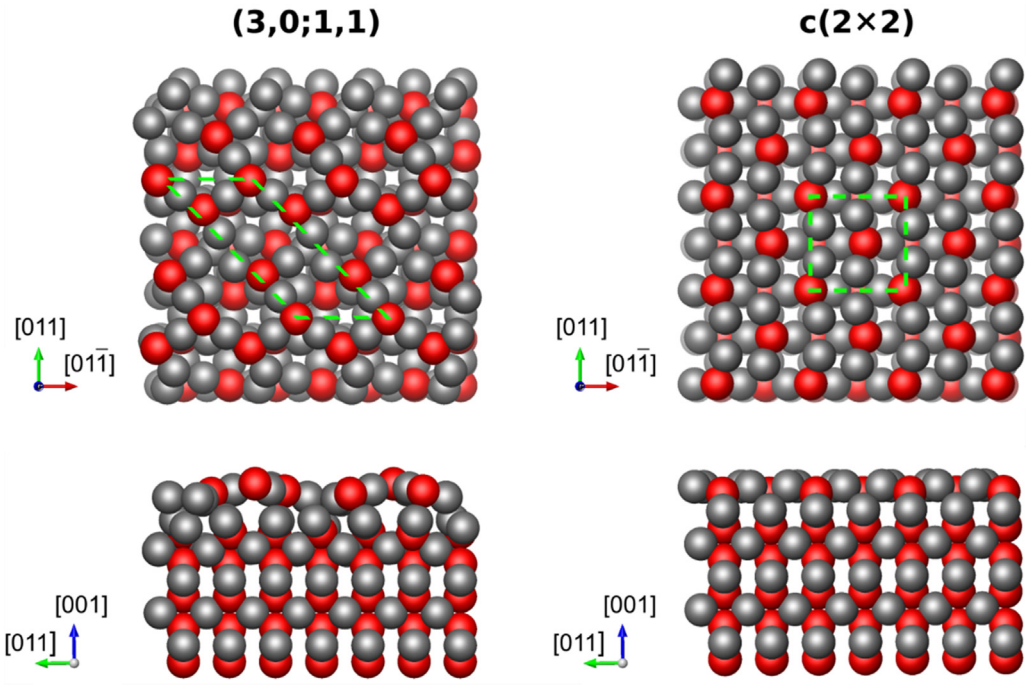

Fig. 8. Surface structures of the (3,0;1,1) and c(2 × 2) surface models of Cu-terminated $Cu_2O(100)$. Copper in grey, oxygen in red. Unit cells indicated by green dashed lines. (For interpretation of the references to colour in this figure legend, the reader is referred to the web version of this article.)

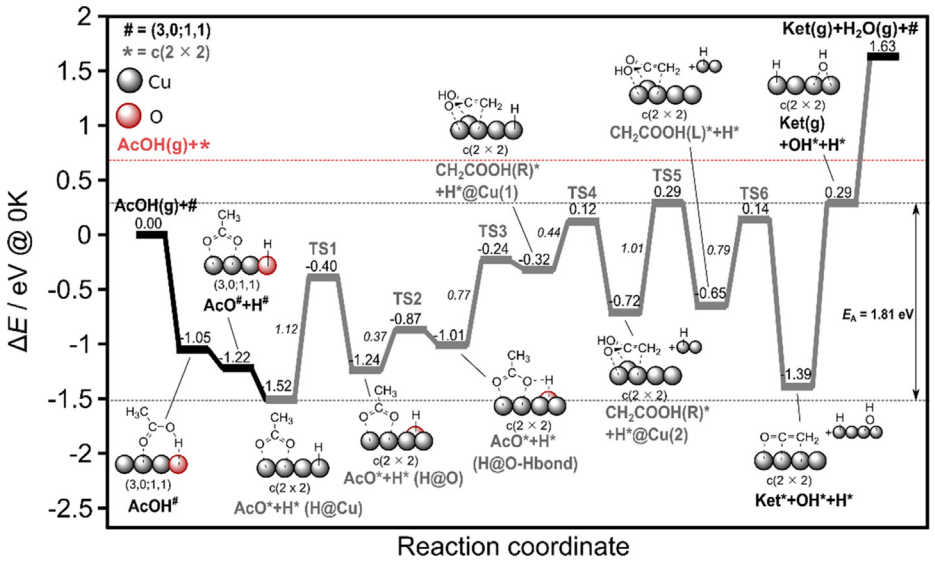

Fig. 9. Mechanism for the acetic acid conversion to ketene over $Cu_2O(100)$ modeled at the PBE-D3+U level of theory. Gibbs free energies at 600 K and 10^{-10} bar included in Fig. S13.

computationally by Wang et al. on the TiO_2 and ZrO_2 surfaces, the formation of ketene* from acetate* first goes via the reprotonation of the acetate* into acetic acid* [52]. Fig. 9 shows that this step is uphill by 0.51 eV, with a barrier of 1.12 eV. On $Cu_2O(100)$, the reprotonated state is in-fact an acetate H-bonded to a surface OH group. In order to accommodate for this structure, a H* has to diffuse from a Cu bridge site to an O-site. This diffusion accounts for the barrier of 1.12 eV. H-diffusion between Cu bridge sites has a lower barrier of only 0.80 eV. See Figs. 10 and 11 for adsorbate and transition state structures.

From the H-bonded structure, the acetate adsorbs the H-bonded H and loses a H from the methyl group in a consecutive step. Also, this step is uphill by 0.69 eV, and the barrier is 0.77 eV. In this structure, the CH_2COOH* intermediate lies flat on the surface binding to four surface Cu via all the C and O atoms. The dissociated H resides at a Cu bridge site close to the CH_2-group. Its diffusion to a distant Cu-bridge site is swift, with a barrier of 0.44 eV (lower than normal diffusion), and exothermic by −0.40 eV.

In order to prepare for the final step to generate ketene - i.e., dissociation of the C—OH bond of CH_2COOH* intermediate – the H on the OH has to shift from one O to the other. This can be achieved either via molecular rotation, deprotonation, and abstraction of a surface H or via internal H-transfer. The latter has a barrier of 1.01 eV and is close to thermoneutral (the energy difference is here +0.07 eV). With this mechanism, the total barrier of the ketene formation is 1.81 eV. The subsequent dissociation to ketene

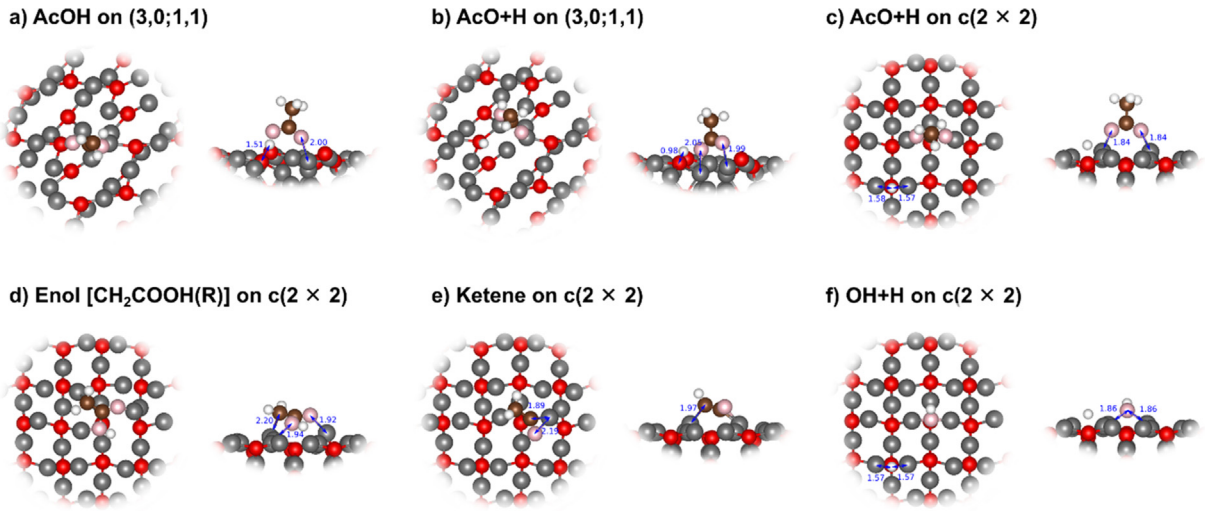

Fig. 10. Adsorbate structures for the ketene formation mechanism from acetic acid on $Cu_2O(100)$. Copper in grey, lattice oxygen in red, adsorbed oxygen in pink, carbon in brown, and hydrogen in white. Distances in Å. (For interpretation of the references to colour in this figure legend, the reader is referred to the web version of this article.)

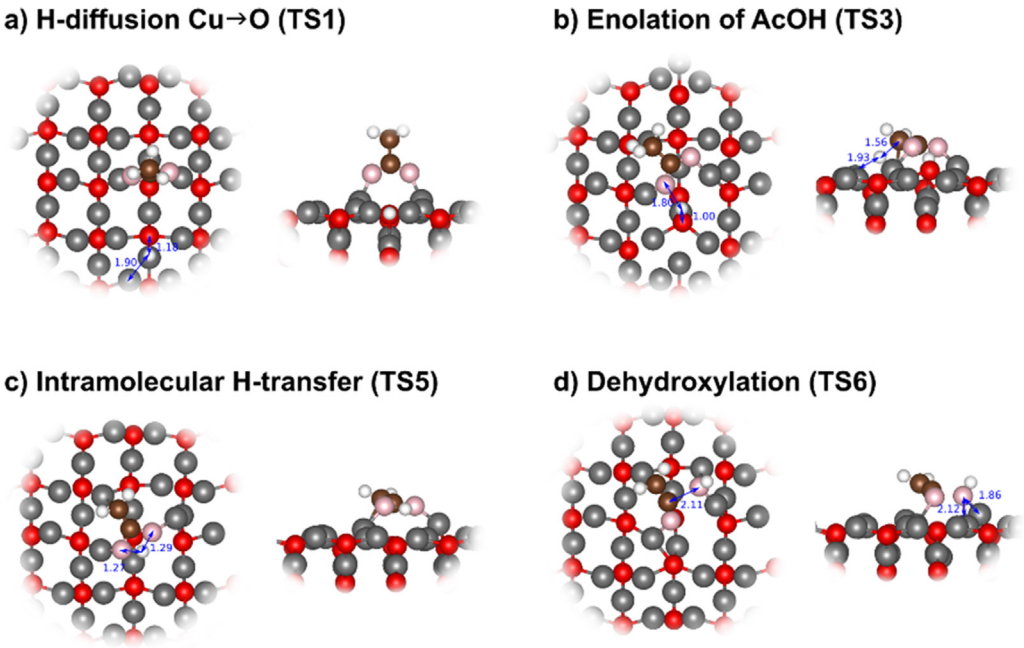

Fig. 11. Transition state structures for the ketene formation mechanism from acetic acid on $Cu_2O(100)$. Copper in grey, lattice oxygen in red, adsorbed oxygen in pink, carbon in brown, and hydrogen in white. Distances in Å. (For interpretation of the references to colour in this figure legend, the reader is referred to the web version of this article.)

and OH* is exothermic by −0.74 eV with a barrier of 0.79 eV. This barrier is not rate-limiting, as its energy with respect to the lowest energy structure on the surface (i.e. acetate with H* at a Cu-bridge site) is 1.66 eV. In the resulting structure, ketene* binds via all C and O atoms to surface Cu atoms in agreement with the experimental predicted structure of the reaction intermediate, whereas H* and OH* both sit at Cu-bridge sites. Ketene* co-adsorbed with H* and OH* is 0.13 eV endothermic compared to acetate* + H*.

Desorption of both ketene and water from the surface will lead to the regeneration of the (3,0;1,1) surface reconstruction. This is also observed experimentally: the typical ridge structure corresponding to (3,0;1,1) reappears in the STM images (Fig. S7) and the low-energy finger-print region in the O 1s XPS spectrum is regained. The individual desorption enthalpy of ketene from c (2 × 2) leading to a gaseous ketene and the (3,0;1,1) surface is 0.96 eV. The corresponding energy for associative desorption of water is 1.34 eV. Depending on the available thermal energy, these may leave in any order from the surface. Adding the desorption energies together and making a balanced account for the surface reconstruction energy (as the ketene*+H*+OH* adsorbates should be attributed to the same (3,0;1,1)-unit, the reconstruction energy can only be included once), the total desorption enthalpy from ketene*+H*+OH* is 3.02 eV. This leaves the gas-phase products at 1.63 eV, which is also the reaction enthalpy. The reader is reminded that this is at 0 K, explaining the difference in reaction enthalpy, ΔH°_{R}, reported earlier for the reaction at 300 K (i.e. ΔH°_{R}, = 1.43 eV).

Accounting for thermal effects in the DFT results leads to a shift in the reaction free energies. As the temperature rises, forming ketene and water becomes more favorable because we change

the number of gas-phase molecules. At 300 K, the ΔG°_{R} is 0.97 eV, and at 600 K ΔG_R = 0.34 eV. At the ultra-low pressures in the experiments (~10^{-10} bar), the reaction is exergonic at 600 K with ΔG_R = −0.85 eV. Thus, the seemingly high barrier for desorption is pushed to favorable energetics at the studied reaction conditions. Hence, the limiting factor for ketene generation is the high barrier for the conversion.

The DFT results can be compared to the TPD data of acetic acid in Fig. 6b. For ketene desorption, the desorption peak maximum appears at ~630 K. Solving the Redhead equation using the TPD scan rate of 3 K/s and assuming a pre-exponential factor of 10^{13} Hz [59], the corresponding desorption energy is 1.74 eV. This is not far away from the computed reaction barrier of 1.81 eV, and within the computational error of the employed methods. The half-life for a first order reaction with a 1.81 eV barrier at 630 K is 15.9 s, which is comparable to the desorption rate in the TPD data. All in all, the main reaction path at elevated temperature (>600 K) for acetic acid conversion over $Cu_2O(100)$ seems to be the transformation into ketene and water. Minor production of CO, CO_2 is also seen on the surface. From the TPD results, we estimate that ketene coverage is around 0.15 ML, which is in a fair agreement with the DFT calculations.

5. Conclusions

We employ a combination of STM, LEED, TPD, XPS, and DFT to describe the decomposition mechanisms of formic and acetic acids on the $Cu_2O(100)$ surface. Adsorption on clean and pre-hydroxylated surfaces was investigated at two acid pressure ranges (10^{-9}-10^{-8} mbar and 10^{-2} mbar). The observed results are similar in all cases, suggesting that surface hydroxyls and acid pressure during dosing are not critical parameters for the reaction. XPS and TPD observations suggest that both acids react with the surface through deprotonation to form formate* and acetate* species bonded to surface copper atoms and hydrogen* atoms bonded to nearby surface oxygen atoms. At increasing surface temperature formate* decompose and results in desorption of CO_2 and CO, as confirmed by TPD. In the case of acetic acid, the picture is more complex, in addition to CO and CO_2 desorption, a third reaction path leads to the formation of large yields of ketene. Of interest to the CO_2 desorption is the observation of an intermediate $CO_2^{\delta-}$ surface species by XPS. The low proportions of H_2 product, as seen in the TPD analysis, and the formation of metallic Cu clusters observed by STM and Auger spectroscopy, suggest that decomposition reactions include abstraction of surface oxygen atoms. The ketene formation reaction mechanism, specific to acetic acid, was modeled by DFT. DFT confirms the strong interaction of acetic acid with the (3,0;1,1) surface and the spontaneous dissociation into acetate* and H*, the latter forming an OH-group at a nearby oxygen site. The surface experiences a local reorganization to the $c(2 \times 2)$ reconstruction to better accommodate the adsorbates due to an enhanced flexibility of surface Cu atoms in this reconstruction. The surface reorganization remains local and is restricted to the vicinity of the adsorbate. The suggested mechanism sets the total barrier for ketene formation to 1.81 eV. The reaction intermediate consists of a ketene* molecule bonded via all C and O atoms to surface Cu atoms, in agreement with the XPS results. The ketene desorption energy estimated from TPD is 1.74 eV, which is not far away from the computed reaction barrier of 1.81 eV and within the computational error of the employed methods, supporting the model mechanism. Our experimental observations, in agreement with mechanistic DFT studies, present a detailed reaction mechanism for ketene formation and suggests that Cu_2O can operate as an efficient catalyst for green generation of ketene from acetic acid.

6. Author information

Present address: H. Tissot, now at CINaM, UMR 7325, Aix-Marseille Univ., CNRS, F-13288, Marseille, France; J. H. Stenlid now at the SUNCAT Center for Interface Science and Catalysis, SLAC National Accelerator Laboratory, 2575 Sand Hill Road, Menlo Park, CA 94025, United States, and Department of Chemical Engineering, Stanford University, 443 Via Ortega, Stanford, CA 94305, United States. F. Johansson now at Institut für Physik und Astronomie, Universität Potsdam, 14476, Potsdam, Germany and Institute for Methods and Instrumentation for Synchrotron Radiation Research, Helmholtz-Zentrum Berlin für Materialien und Energie GmbH, 12489, Berlin, Germany.

Declaration of Competing Interest

The authors declare that they have no known competing financial interests or personal relationships that could have appeared to influence the work reported in this paper.

Acknowledgement

Milad Ghadami Yazdi and Matthias Muntwiler are kindly acknowledged for their assistance during the beamtime at PEARL. This work was funded by the Swedish Research Council (VR), the Knut och Alice Wallenbergs stiftelse, and STINT Joint China-Sweden Mobility program. HT acknowledge the financial support from the Ragnar Holm foundation, CW the financial support from Trygger's foundation. YS acknowledges funding from VR with a Starting Grant (Dnr. 2017-05078) and Chalmers Areas of Advance-Materials Science. The SLS staff is gratefully acknowledged for their support during beamtimes. SK thanks to TARLA for collaborative research effort. The computations were carried out on resources provided by the Swedish National Infrastructure for Computing (SNIC) at the PDC Center for High Performance Computing, KTH Royal Institute of Technology.

Appendix A. Supplementary material

The supporting information includes additional XPS results and analysis, complementing STM and TPD data as well as DFT results. Supplementary data to this article can be found online at https://doi.org/10.1016/j.jcat.2021.08.022.

References

[1] M. Hara, T. Kondo, M. Komoda, S. Ikeda, K. Shinohara, A. Tanaka, J.N. Kondo, K. Domen, M. Hara, K. Shinohara, A. Tanaka, Cu_2O as a Photocatalyst for Overall Water Splitting under Visible Light Irradiation, Chem. Commun. 2 (1998) 357–358.
[2] D. Barreca, P. Fornasiero, A. Gasparotto, V. Gombac, C. Maccato, T. Montini, E. Tondello, The Potential of Supported Cu_2O and CuO Nanosystems in Photocatalytic H_2 Production, ChemSusChem 2 (2009) 230–233.
[3] K.H. Schulz, D.F. Cox, Propene Adsorption on Cu_2O Single-Crystal Surfaces, Surf. Sci. 262 (1992) 318–334.
[4] B. White, M. Yin, A. Hall, D. Le, S. Stolbov, T. Rahman, N. Turro, S. O'Brien, Complete CO Oxidation over Cu_2O Nanoparticles Supported on Silica Gel, Nano Lett. 6 (2006) 2095–2098.
[5] Z. Besharat, J.H. Stenlid, M. Soldemo, K. Marks, A. Önsten, M. Johnson, H. Öström, J. Weissenrieder, T. Brinck, M. Göthelid, Dehydrogenation of Methanol on Cu_2O (100) and (111), J. Mater. Chem. 146 (2017) 244702.
[6] Y.A. Wu, I. McNulty, C. Liu, K.C. Lau, Q. Liu, A.P. Paulikas, C.J. Sun, Z. Cai, J.R. Guest, Y. Ren, V. Stamenkovic, L.A. Curtiss, Y. Liu, T. Rajh, Facet-Dependent Active Sites of a Single Cu_2O Particle Photocatalyst for CO_2 Reduction to Methanol, Nat. Energy 4 (2019) 957–968.
[7] C. Leygraf, I.O. Wallinder, J. Tidblad, T.E. Graedel, Atmospheric Corrosion, John Wiley & Sons, 2016.
[8] M. Bowker, R.J. Madix, The Adsorption and Oxidation of Acetic Acid and Acetaldehyde on Cu(110), Appl. Surf. Sci. 8 (1981) 299–317.
[9] F.S. Wagner, Acetic Anhydride, John Wiley & Sons, 2002.

[10] C.D. Hurd, K.E. Martin, Ketene from Acetic Acid, J. Am. Chem. Soc. 51 (1929) 3614–3617.
[11] E. Peytral, The Mode of Sudden Pyrogenic Decomposition of Acetic Acid at High Temperature, Bull. Soc. Chim. 31 (1922) 113.
[12] R. Milller, C. Abaecherli, A. Said, J.B. Ketenes, Ullmann's Encyclopedia Ind. Chem. (2012).
[13] E.J. Grootendorst, R. Pestman, R.M. Koster, V. Ponec, Selective Reduction of Acetic Acid to Acetaldehyde on Iron Oxides, J. Catal. 148 (1994) 261–269.
[14] F.C. Calaza, T.-L. Chen, D.R. Mullins, Y. Xu, S.H. Overbury, Reactivity and Reaction Intermediates for Acetic Acid Adsorbed on CeO_2(111), Catal. Today 253 (2015) 65–76.
[15] S.V. Chong, H. Idriss, Reactions of Acetic Acid on UO_2(111) Single Crystal Surfaces, J. Vac. Sci. Technol. A 18 (2000) 1900–1904.
[16] J. Stubenrauch, E. Brosha, J.M. Vohs, Reaction of Carboxylic Acids on CeO_2(111) and CeO_2(100), Catal. Today 28 (1996) 431–441.
[17] K.S. Kim, M.A. Barteau, Structure and Composition Requirements for Deoxygenation, Dehydration, and Ketonization Reactions of Carboxylic Acids on TiO2 Single Crystal Surfaces, J. Catal. 125 (1990) 353–375.
[18] M.C. Libby, P.C. Watson, M.A. Barteau, Synthesis of Ketenes with Oxide Catalysts, Ind. Eng. Chem. Res. 33 (1994) 2904–2912.
[19] Y. Zhang, D.R. Mullins, A. Savara, Effect of Sr Substitution in $LaMnO_3$(100) on Catalytic Conversion of Acetic Acid to Ketene and Combustion-like Products, J. Phys. Chem. C 123 (2019) 4148–4157.
[20] I. Lyubinetsky, N.A. Deskins, Y. Du, E.K. Vestergaard, D.J. Kim, M. Dupuis, Adsorption States and Mobility of Trimethylacetic Acid Molecules on Reduced TiO_2(110) Surface, Phys. Chem. Chem. Phys. 12 (2010) 5986–5992.
[21] G. Pacchioni, Ketonization of Carboxylic Acids in Biomass Conversion over TiO_2 and ZrO_2 Surfaces: A DFT Perspective, ACS Catal. 4 (2014) 2874–2888.
[22] J. Tao, T. Luttrell, J. Bylsma, M. Batzill, Adsorption of Acetic Acid on Rutile TiO_2(110) vs (011)-2×1 Surfaces, J. Phys. Chem. C 115 (2011) 3434–3442.
[23] C.M. Dover, D.C. Grinter, C.M. Yim, C.A. Muryn, H. Bluhm, M. Salmeron, G. Thornton, Orientation of Acetic Acid Hydrogen Bonded to Acetate Terminated TiO_2(110), Surf. Sci. 699 (2020) 121628.
[24] E.L. Quah, J.N. Wilson, H. Idriss, Photoreaction of the Rutile TiO_2(011) Single-Crystal Surface: Reaction with Acetic Acid, Langmuir 26 (2010) 6411–6417.
[25] B.A. Sexton, Observation of Formate Species on a Copper (100) Surface by High Resolution Electron Energy Loss Spectroscopy, Surf. Sci. 88 (1979) 319–330.
[26] M. Bowker, R.J. Madix, XPS, UPS and Thermal Desorption Studies of the Reactions of Formaldehyde and Formic Acid with the Cu(110) Surface, Surf. Sci. 102 (1981) 542–565.
[27] S.A. Chambers, M.A. Henderson, Y.J. Kim, S. Thevuthasan, Chemisorption Geometry, Vibrational Spectra, and Thermal Desorption of Formic Acid on TiO_2(110), Surf. Rev. Lett. 5 (1998) 381–385.
[28] Y. Wang, B. Wen, A. Dahal, G.A. Kimmel, R. Rousseau, A. Selloni, N.G. Petrik, Z. Dohnálek, Binding of Formic Acid on Anatase TiO_2(101), J. Phys. Chem. C 124 (2020) 20228–20239.
[29] Markus Soldemo, Joakim Halldin Stenlid, Zahra Besharat, Milad Ghadami Yazdi, Anneli Önsten, Christofer Leygraf, Mats Göthelid, Tore Brinck, Jonas Weissenrieder, The Surface Structure of Cu_2O(100), J. Phys. Chem. C 120 (8) (2016) 4373–4381.
[30] H. Tissot, C. Wang, J.H. Stenlid, T. Brinck, J. Weissenrieder, The Surface Structure of Cu_2O(100): Nature of Defects, J. Phys. Chem. C 123 (2019) 7696–7704.
[31] M. Muntwiler, J. Zhang, R. Stania, F. Matsui, P. Oberta, U. Flechsig, L. Patthey, C. Quitmann, T. Glatzel, R. Widmer, E. Meyer, T.A. Jung, P. Aebi, R. Fasel, T. Greber, Surface Science at the PEARL Beamline of the Swiss Light Source, J. Synchrotron Rad 24 (2017) 354–366.
[32] G. Kresse, Efficient Iterative Schemes for Ab Initio Total-Energy Calculations Using a Plane-Wave Basis Set, Phys. Rev. B 54 (1996) 11169–11186.
[33] J.P. Perdew, K. Burke, M. Ernzerhof, Generalized Gradient Approximation Made Simple, Phys. Rev. Lett. 77 (1996) 3865–3868.
[34] S. Grimme, S. Ehrlich, L. Goerigk, Effect of the Damping Function in Dispersion Corrected Density Functional Theory, J. Comput. Chem. 32 (2011) 1456–1465.
[35] S. Grimme, J. Antony, S. Ehrlich, H. Krieg, A Consistent and Accurate Ab Initio Parametrization of Density Functional Dispersion Correction (DFT-D) for the 94 Elements H-Pu, J. Chem. Phys. 132 (2010) 154104.
[36] S.L. Dudarev, G.A. Botton, S.Y. Savrasov, C.J. Humphreys, A.P. Sutton, Electron-Energy-Loss Spectra and the Structural Stability of Nickel Oxide: An LSDA+U Study, Phys. Rev. B 57 (1998) 1505–1509.
[37] G. Kresse, D. Joubert, From Ultrasoft Pseudopotentials to the Projector Augmented-Wave Method, Phys. Rev. B 59 (1999) 1758–1775.
[38] P.E. Blöchl, Projector Augmented-Wave Method, Phys. Rev. B 50 (1994) 17953–17979.
[39] P.E. Blöchl, O. Jepsen, O.K. Andersen, Improved Tetrahedron Method for Brillouin-Zone Integrations, Phys. Rev. B 49 (1994) 16223–16233.
[40] L. Köhler, G. Kresse, Density Functional Study of CO on Rh(111), Phys. Rev. B 70 (2004) 1–9.
[41] V. Nilsson, M. Van Den Bossche, A. Hellman, H. Grönbeck, Trends in Adsorbate Induced Core Level Shifts, Surf. Sci. 640 (2015) 59–64.
[42] M.J. Frisch, G.W. Trucks, H.B. Schlegel, G.E. Scuseria, M.A. Robb, J.R. Cheeseman, G. Scalmani, V. Barone, G.A. Petersson, H. Nakatsuji, X. Li, M. Caricato, A.V. Marenich, J. Bloino, B.G. Janesko, R. Gomperts, B. Mennucci, H.P. Hratchian, V.J., D.J. Fox, Gaussian 16, Revision C.01. Gaussian, Inc., Wallingford CT, 2016.
[43] J.H. Stenlid, M. Soldemo, A.J. Johansson, C. Leygraf, M. Göthelid, J. Weissenrieder, T. Brinck, Reactivity at the Cu_2O(100):Cu–H_2O Interface: A Combined DFT and PES Study, Phys. Chem. Chem. Phys. 18 (2016) 30570–30584.
[44] H. Tissot, C. Wang, J.H. Stenlid, M. Panahi, S. Kaya, M. Soldemo, M. Ghadami Yazdi, T. Brinck, J. Weissenrieder, Interaction of Atomic Hydrogen with the Cu_2O(100) and (111) Surfaces, J. Phys. Chem. C 123 (2019) 22172–22180.
[45] Y. Yao, F. Zaera, Adsorption and Thermal Chemistry of Formic Acid on Clean and Oxygen-Predosed Cu(110) Single-Crystal Surfaces Revisited, Surf. Sci. 646 (2016) 37–44.
[46] M. Bowker, E. Rowbotham, F.M. Leibsle, S. Haq, The Adsorption and Decomposition of Formic Acid on Cu(110), Surf. Sci. 349 (1996) 97–110.
[47] M. Bowker, C. Morgan, J. Couves, Acetic Acid Adsorption and Decomposition on Pd(110), Surf. Sci. 555 (2004) 145–156.
[48] J.M. Vohs, M.A. Baretau, Reaction Pathways and Intermediates in the Decomposition of Aceticand Propionic Acids on the Polar Surface of Zinc Oxide, Surf. Sci. 201 (1988) 481–502.
[49] X. Deng, A. Verdaguer, T. Herranz, C. Weis, H. Bluhm, M. Salmeron, Surface Chemistry of Cu in the Presence of CO_2 and H_2O, Langmuir 24 (2008) 9474–9478.
[50] S. Poulston, E. Rowbotham, P. Stone, P. Parlett, M. Bowker, Temperature-Programmed Desorption Studies of Methanol and Formic Acid Decomposition on Copper Oxide Surfaces, Catal. Letters 52 (1998) 63.
[51] D.H.S. Ying, R.J. Madix, Thermal Desorption Study of Formic Acid Decomposition on a Clean Cu(110) Surface, J. Catal. 61 (1980) 48–56.
[52] S. Wang, E. Iglesia, Experimental and Theoretical Assessment of the Mechanism and Site Requirements for Ketonization of Carboxylic Acids on Oxides, J. Catal. 345 (2017) 183–206.
[53] P.L. Radloff, G.E. Mitchell, C.M. Greenlief, J.M. White, The Surface Chemistry of Ketene on Pt(111), Surf. Sci. 183 (1987) 377–402.
[54] A.A. Gokhale, J.A. Dumesic, M. Mavrikakis, On the Mechanism of Low-Temperature Water Gas Shift Reaction on Copper, J. Am. Chem. Soc. 130 (2007) 1402–1414.
[55] Nist webbook: https://webbook.nist.gov/chemistry/ accessed 2020-06-04.
[56] K. Tanaka, M. Yoshimine, An Ab Initio Study on Ketene, Hydroxyacetylene, Formylmethylene, Oxirene, and Their Rearrangement Paths, J. Am. Chem. Soc. 102 (1980) 7656–7662.
[57] K. Marks, Z. Besharat, M. Soldemo, A. Önsten, J. Weissenrieder, J.H. Stenlid, H. Öström, M. Göthelid, Adsorption and Decomposition of Ethanol on Cu_2O(111) and (100), J. Phys. Chem. C 123 (2019) 20384–20392.
[58] C. Liu, J.H. Stenlid, L.G.M. Pettersson, Amorphous, Periodic Model of a Copper Electrocatalyst with Subsurface Oxygen for Enhanced CO Coverage and Dimerization, J. Phys. Chem. C 123 (2019) 4961–4968.
[59] A.M. De Jong, J.W. Niemantsverdriet, Thermal Desorption Analysis: Comparative Test of Ten Commonly Applied Procedures, Surf. Sci. 233 (1990) 355–365.